

See discussions, stats, and author profiles for this publication at: <https://www.researchgate.net/publication/257927923>

Quantification of Al-goethite from diffuse reflectance spectroscopy and magnetic methods

Article in *Geophysical Journal International* · October 2013

DOI: 10.1093/gji/gg1377

CITATIONS

7

READS

285

6 authors, including:



Zhaoxia Jiang

Ocean University of China

43 PUBLICATIONS 308 CITATIONS

[SEE PROFILE](#)



Qingsong Liu

Department of Ocean Science and Engineering

205 PUBLICATIONS 5,544 CITATIONS

[SEE PROFILE](#)



Claudio Colombo

Università degli Studi del Molise

69 PUBLICATIONS 1,247 CITATIONS

[SEE PROFILE](#)



Vidal Barrón

University of Cordoba (Spain)

179 PUBLICATIONS 4,618 CITATIONS

[SEE PROFILE](#)

Some of the authors of this publication are also working on these related projects:



Color and uv-vis-nir spectroscopy of Fe minerals [View project](#)



the National Natural Science Foundation of China [View project](#)

Quantification of Al-goethite from diffuse reflectance spectroscopy and magnetic methods

Zhaoxia Jiang,^{1,2} Qingsong Liu,¹ Claudio Colombo,³ Vidal Barrón,⁴ José Torrent⁴ and Pengxiang Hu^{1,2}

¹State Key Laboratory of Lithospheric Evolution, Institute of Geology and Geophysics, Chinese Academy of Sciences, Beijing 100029, China.
E-mail: liux0272@yahoo.com

²University of the Chinese Academy of Sciences, Beijing 100049, China

³Università del Molise Dip. di Agricoltura, Alimentazione ed Ambiente, v. De Sanctis, I-86100 Campobasso (CB), Italy

⁴Departamento de Agronomía, Universidad de Córdoba, Edificio C4, Campus de Rabanales, E-14071 Córdoba, Spain

Accepted 2013 September 16. Received 2013 August 27; in original form 2013 March 28

SUMMARY

As one of the most abundant iron oxides in soils, the presence and nature of goethite is controlled by the soil conditions and burial history. The visible diffuse reflectance spectroscopy (DRS) is a useful tool for quantifying goethite. However, aluminium (Al) substitution for goethite is very common in soils and the effects of Al content on the DRS properties of goethite have not been fully resolved. In this study, two series of Al substituted goethites (Al-goethite) and 20 Chinese loess/palaeosol samples were investigated using both DRS and magnetic methods to test the feasibility of quantifying Al-goethite with the DRS method. Results show that the peak positions and amplitudes of the goethite DRS band are significantly influenced by Al substitution. Specifically, the goethite concentration proxy, the amplitude of the DRS band, is relatively stable only when Al substitution ranged between about 4 and 16 mol per cent. Practically, in order to resolve the difficulty in measuring Al content in natural samples, the unblocking temperature (T_b) is proposed as the proxy for Al substitution of goethite. When T_b of Al-goethite was above 250 K, the amplitude of DRS can be used to reliably trace the goethite concentration variation in natural samples. For example, the DRS spectra for the Chinese loess–palaeosol samples support the idea that only haematite is enhanced via pedogenesis. In contrast, the origin of goethite seems to be mostly related to the aeolian inputs.

Key words: Environmental magnetism; Magnetic mineralogy and petrology; Rock and mineral magnetism.

1 INTRODUCTION

Goethite (α -FeOOH) is one of the most abundant iron oxides in soils from many climatic areas, although a minor carrier of stable palaeomagnetic remanence (Banerjee 1970; Dekkers & Rochette 1992; Cornell & Schwertmann 2003; Evans & Heller 2003). The presence and characteristics of goethite are indicators for soil-weathering conditions and burial history (Balsam *et al.* 2004). The haematite (α -Fe₂O₃) to (haematite + goethite) ratio [Hm/(Hm + Gt)] depends primarily on the parent minerals, soil environment and the duration of pedogenesis (Cornell & Schwertmann 2003). Climate governs the pedogenetic formation rate and the ratio of haematite to goethite since these minerals are formed under opposite climate conditions (dry and warm for haematite, wet and cool for goethite) and their formation processes are competitive (Schwertmann 1993). In particular, this ratio remains stable for a very long period unless these phases are reductively dissolved, and

thus can provide important information for soil moisture related with climate changes (Kämpf & Schwertmann 1983; Schwertmann 1987; Balsam *et al.* 2004; Ji *et al.* 2004; Zhang *et al.* 2007). However, it is very difficult to determine the concentration of these two minerals in soil and sediments. As an antiferromagnetic mineral, the Néel temperature (T_N) of goethite is around 120 °C (Özdemir & Dunlop 1996; Mathé *et al.* 1999; Liu *et al.* 2004, 2006), but the coercivity of goethite is sometimes too high to be detected by more conventional rock magnetic methods (Rochette *et al.* 2005), so new methods are urgently needed.

Diffuse reflectance spectroscopy (DRS) in the visible (VIS, ~400–700 nm) and near infrared (NIR) range (~700–2500 nm) have been used in the identification and semi-quantification of goethite and haematite in soils (Cornell & Schwertmann 2003; Balsam *et al.* 2004; Ji *et al.* 2004; Torrent *et al.* 2007), aerosols (Shen *et al.* 2006; Lázaro *et al.* 2008) and sediments (Balsam & Deaton 1996; Zhang *et al.* 2007). The

reflectance of soils and sediments includes two components, ‘specular reflectance’ and ‘diffuse reflectance’. When a beam of incident light impinges on the surface of a kind of powdered material, only a small fraction is specularly reflected, which is ‘specular reflectance’, and the remainder penetrates into the mass and undergoes scattering (namely, multiple reflections, refractions and diffractions in all directions) and wavelength-dependent absorption within the coloured materials. Part of this radiation ultimately leaves the material in all directions and constitutes so-called ‘diffusely reflectance’ (Torrent & Barrón 2002, 2008). Differently coloured iron oxides display different reflecting behaviour. Thus, the analysis of corresponding ‘diffuse reflectance spectra’ has been proved useful to identify and characterize different types of iron oxides, especially for haematite and goethite, whose detection limit is about 5 g kg^{-1} , one order of magnitude lower than that of X-ray diffraction (XRD) analysis (Torrent *et al.* 1983; Kosmas *et al.* 1984, 1986).

The colour parameters derived directly from DRS have been used to estimate the content of haematite and goethite in soils and sediments (Torrent *et al.* 1983; Barrón & Torrent 1986; Ji *et al.* 2001, 2002). Actually the colour of synthetic haematite is related to the position and/or intensity of the main absorption bands in the visible spectrum, occurring at ~ 435 , ~ 485 and ~ 535 nm. The properties of the band at 535 nm seem to be influenced by the degree of aluminium (Al) substitution and the specific surface area of haematite, whereas the crystal properties seem to influence the properties of the two other bands (Torrent & Barrón 2003; Liu *et al.* 2011). To enhance the resolution, Deaton & Balsam (1991) calculated the first derivative of the original DRS, and obtained the characteristic peaks for goethite and haematite, the intensity of which can be used to measure the content of goethite and haematite. However, Kosmas *et al.* (1984, 1986) and Scheinost *et al.* (1998) used the second derivative to detect and quantify different iron oxides in soils and sediments. Torrent & Barrón (2002) proposed that the second-derivative curve can provide more information than the first-derivative curve does. In practice, the first- and second-derivative curves of DRS spectra, are both widely used as ‘fingerprint’ for iron oxides in soils and sediments (Kosmas *et al.* 1984; Balsam *et al.* 2004; Torrent *et al.* 2007; Hao *et al.* 2009).

For goethite, the minimum at 435 nm in the first-derivative curve and the minimum at 425 nm in the second-derivative curve are characteristic peaks of this mineral, which can be assigned to the ${}^6\text{A}_1({}^6\text{S}) \rightarrow {}^4\text{A}_1({}^4\text{G})$ transition (Kosmas *et al.* 1984, 1986; Sherman & Waite 1985; Scheinost *et al.* 1998). The intensity of these peaks can be used for the quantification of goethite (Kosmas *et al.* 1984;

Balsam *et al.* 2004; Torrent *et al.* 2007; Hao *et al.* 2009). However, goethite is usually Al-substituted in natural environments, which can reach up to 33 mol per cent (Taylor & Schwertmann 1978; Lewis & Schwertmann 1979; Schulze 1984). Al substitution plays a dramatic role on the properties of goethite, such as magnetic properties (Murad & Bowen 1987; Kilcoyne & Ritter 1997; Liu *et al.* 2004, 2006), unit cell parameters (Schulze 1984; Cornell & Schwertmann 2003; Liu *et al.* 2006), morphology (Schulze & Schwertmann 1984; Mann *et al.* 1985) and visible DRS and colour parameters (Kosmas *et al.* 1986). Therefore, Al substitution may influence the position and intensity of the characteristic DRS peak. However, Kosmas *et al.* (1986) and Scheinost *et al.* (1999) showed that the 447 nm maximum and 425 nm minimum in the second-derivative curve do not change with Al substitution, although the position of the minimum at 480 nm is more sensitive to Al substitution, which shifts to lower wavelength as Al content increases.

In order to investigate the sensitivity of goethite DRS to Al substitution and the feasibility for quantification of goethite with DRS, two series of Al-goethite samples and 20 Chinese loess/palaeosol samples were investigated using both DRS and magnetic methods.

2 MATERIAL AND METHODS

Two series of goethites were hydrothermally synthesized via different methods as described by Jiang *et al.* (2012). Series GtIII* samples [GtIII0, GtIII2, GtIII4, GtIII8, GtIII16, GtIII20, GtIII30, where GtIII stands for goethite transformed from Fe(III) salt, and the number represents the initial Al content in the solution] were prepared by aging $\text{Fe}(\text{NO}_3)_3$ and $\text{Al}(\text{NO}_3)_3$ solutions to which 5 mol L^{-1} (M) NaOH was added at 60°C , while series GtII* samples [GtII0, GtII4, GtII8, GtII16, GtII20, GtII30, where GtII represents goethite transformed from Fe(II) solution, and the number stands for the initial Al content in the solution] were produced by oxidation of Fe(II) and Al salts at room temperature, adding 0.5 M NaHCO_3 to bring the pH to 7. The products were washed free of other ions by repeated washing with deionized water, and then dried at 60°C (Schwertmann & Cornell 2000). The final Al concentrations of the solid samples were measured with atomic absorption spectroscopy after dissolving samples into concentrated hydrochloric acid (HCl). Detailed information on the samples is summarized in Table 1.

In order to confirm the purity of these samples, XRD patterns were measured with a Siemens D5000 diffractometer (Japan instrument) monochromatized $\text{CoK}\alpha$ radiation, a step size of $0.05^\circ 2\theta$ and a counting time of 20 s.

Table 1. Methods used to synthesized the goethite samples.

Sample	Procedure and solution used	Aging temperature ($^\circ\text{C}$)	Initial Al content added (mol per cent)	Al content in final samples (mol per cent)	T_b (K)
GtIII0	100 mL 0.6 mol L^{-1} $\text{Fe}(\text{NO}_3)_3$ + 1 mol L^{-1} NaOH	60	0	0	370
GtIII2	100 mL 0.6 mol L^{-1} (Fe, Al)(NO_3) ₃ + 1 mol L^{-1} NaOH	60	2	0.8	360
GtIII4	100 mL 0.6 mol L^{-1} (Fe, Al)(NO_3) ₃ + 1 mol L^{-1} NaOH	60	4	1.5	355
GtIII8	100 mL 0.6 mol L^{-1} (Fe, Al)(NO_3) ₃ + 1 mol L^{-1} NaOH	60	8	2.8	345
GtIII16	100 mL 0.6 mol L^{-1} (Fe, Al)(NO_3) ₃ + 1 mol L^{-1} NaOH	60	16	4.3	335
GtIII20	100 mL 0.6 mol L^{-1} (Fe, Al)(NO_3) ₃ + 1 mol L^{-1} NaOH	60	20	5.3	340
GtIII30	100 mL 0.6 mol L^{-1} (Fe, Al)(NO_3) ₃ + 1 mol L^{-1} NaOH	60	30	6.7	330
GtII0	1 L 0.05 mol L^{-1} FeSO_4 + 110 mL 1 mol L^{-1} NaHCO_3	20	0	0	326
GtII4	1 L 0.05 mol L^{-1} (FeSO_4 + $\text{Al}(\text{NO}_3)_3$) + 110 mL 1 mol L^{-1} NaHCO_3	20	4	3.7	326
GtII8	1 L 0.05 mol L^{-1} (FeSO_4 + $\text{Al}(\text{NO}_3)_3$) + 110 mL 1 mol L^{-1} NaHCO_3	20	8	6.4	296
GtII16	1 L 0.05 mol L^{-1} (FeSO_4 + $\text{Al}(\text{NO}_3)_3$) + 110 mL 1 mol L^{-1} NaHCO_3	20	16	15.8	281
GtII20	1 L 0.05 mol L^{-1} (FeSO_4 + $\text{Al}(\text{NO}_3)_3$) + 110 mL 1 mol L^{-1} NaHCO_3	20	20	18	226
GtII30	1 L 0.05 mol L^{-1} (FeSO_4 + $\text{Al}(\text{NO}_3)_3$) + 110 mL 1 mol L^{-1} NaHCO_3	20	30	28.3	145

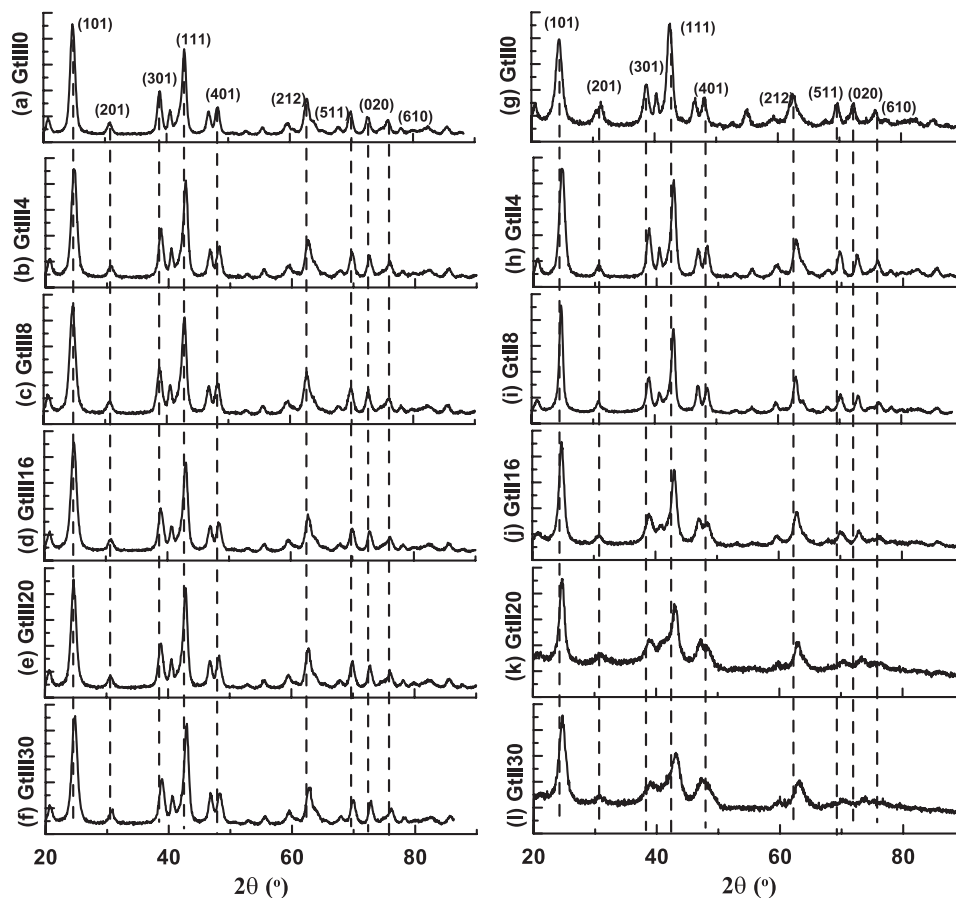


Figure 1. X-ray diffraction spectra of two series of Al-goethite, where the dashed lines and numbers in the brackets are characteristic reflections for goethite.

Scanning electron microscopy (SEM) was carried out using a Zeiss DSM 940 microscope (made in Germany) operating at 20 kV to observe the morphology of the samples. Diluted suspensions were mounted and dried, then sputter coated with gold in a vacuum evaporator. The length and thickness of at least 100 particles were measured for every sample, and then the average values were obtained after Gaussian normal distribution fitting.

The DRS measurements were recorded from 350 to 750 nm in 0.5 nm steps at a scan speed rate of 300 nm min^{-1} using a Varian Cary 5000 spectrophotometer (made in California, USA) equipped with a BaSO_4 -coated integrating sphere and using BaSO_4 as the white standard (Torrent & Barrón 2003, 2008). Samples were carefully packed into a sample holder with a circular hole, and then placed at the side of the integrating sphere vertically. Particle orientation could not be prevented because the powder was pressed against the quartz cover glass of the sample holder. Therefore, particle orientation resulted in part of the incident light being specularly reflected and hence changes in the total (i.e. specularly plus diffusively reflected) light that was collected by the reflectance sphere. In order to account for the variability in the DRS measurement due to differences in particle size orientation caused by differences in packing pressure, samples were poured out after one measurement, packed into the holder again and then tested. In total, each sample was measured 30 times. The DRS data of samples were smoothed using the Varian instrument software (Savitzky–Golay method) with a filtering factor of 5, and then transformed into the Kubelka–Munk (K–M) functions $[(1 - R)^2/2R]$, where R is the reflectance (Torrent & Barrón 2002). The first- and second-derivative curves of these

functions were then derived using that software with a filtering factor of 29.

In order to quantify the Al content of Al-goethite, low-temperature magnetic properties of goethite were measured using a Magnetic Property Measurement System (MPMS XL-5) apparatus. First samples were cooled from room temperature to 10 K in a zero field (ZFC) and a non-zero field (FC), respectively, and then the isothermal remanent magnetization (IRM) was imparted with a 2.5 T field at 10 K. After the magnetic field was switched off, IRM was measured from 10 to 400 K (Liu *et al.* 2004, 2006). In addition, Alternating Current (AC) susceptibility was also measured with frequency of 10 Hz in a 0.4 mT weak field from 10 to 400 K (Mathé *et al.* 1999).

In addition, in order to verify the application of DRS methods to natural samples, the DRS of 20 Chinese loess/palaeosol samples were measured. For natural samples, the magnetic signal of goethite is usually blurred by strongly magnetic minerals. In order to obtain the blocking temperature of goethite in natural samples, the temperature dependence curves of hard isothermal remanent magnetization (HIRM) is measured, which is commonly used to estimate the absolute concentration of haematite and goethite, defined as $(\text{SIRM} + \text{IRM}_{300 \text{ mT}})/2$ (Thompson & Oldfield 1986; Liu *et al.* 2007). For such a definition, HIRM represents the magnetic remanence carried by the magnetic minerals with remanence coercivity $>300 \text{ mT}$, which usually corresponds to the mixture of haematite and goethite. Since haematite in natural samples is almost saturated at 2.5 T field, for this study, HIRM is redefined as $(\text{SIRM} + \text{IRM}_{2.5 \text{ T}})/2$. To avoid the disturbance of the Verwey transition of magnetite

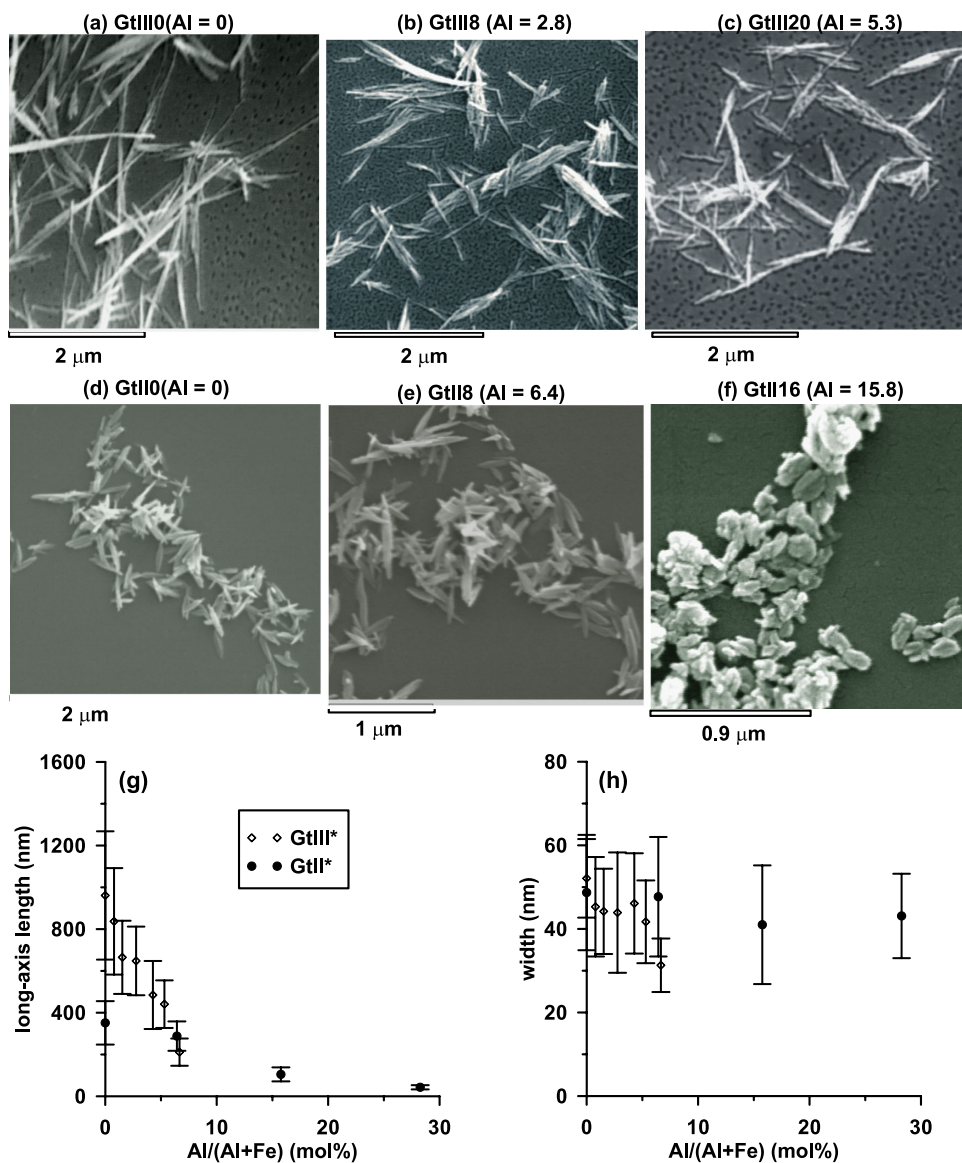


Figure 2. (a–f) Scanning electron micrographs (SEM) of selected samples from these two series samples; (g) the relationship of long-axis length of particles with Al content; (h) the width of goethite particles versus Al content. The parentheses after sample names indicate the Al content in mol per cent.

(~120 K), the temperature dependence of HIRM were measured from 150 to 400 K. First, samples were cooled from the room temperature to 150 K in a zero field (ZFC), and then $SIRM_{5T}$ was imparted with 5 T field. After the magnetic field was switched off, $SIRM_{5T}$ was measured from 150 to 400 K. The curve is defined as $SIRM_{5T}(T)$. After that, samples were cooled to 150 K in a zero field again, and then $IRM_{2.5T}$ was obtained in a 2.5 T backward field, and was thermally demagnetized from 150 to 400 K. The corresponding curve is termed as $IRM_{2.5T}(T)$. For such a treatment, the effects of the Verwey transition (at 120 K) can be ignored. The temperature dependence of HIRM [$HIRM(T)$] is calculated by $[SIRM_{5T}(T) + IRM_{2.5T}(T)]/2$.

3 RESULTS

3.1 XRD and SEM results

The characteristic lattice plane (201), (301), (111), (401) and (212) of goethite in XRD data confirm the purity of the samples; however,

the crystallinity of the sample decreases with increasing Al content (Fig. 1). Distinctive morphologic differences can be observed from the SEM micrographs of the two series goethite samples (Figs 2a–f). For GtIII* series samples, the particles are acicular, while the particles are spindle shaped for GtII* series samples, and become rounded when Al substitution reaches 15.8 mol per cent. In addition, the long-axis lengths of the particle are reverse to Al substitution for both series samples (Fig. 2g), which is consistent with previous studies (Schulze 1984; Liu *et al.* 2006), while the widths are almost constant within standard deviation (Fig. 2h).

3.2 DRS results

The positions of the characteristic bands for the first- (P_{435}) and second- (P_{425}) derivative curves are around 435 nm and 425 nm, respectively. The amplitudes of these characteristic bands, measured as the difference between the minimum at the band and the next associated maximum at longer wavelength in the derivative curves (I_{435} , I_{425}) (Fig. 3), were successfully used to predict

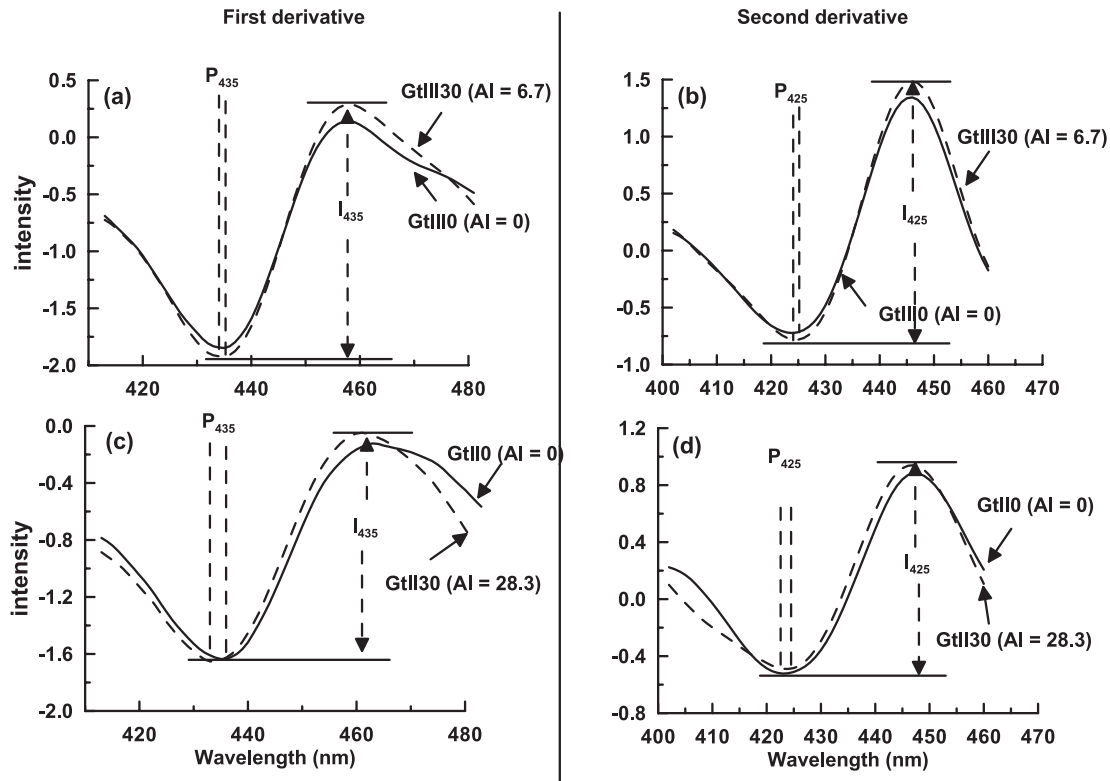


Figure 3. The first- and second-derivative curves of K–M functions for selected samples, where the parentheses after sample names indicate the Al content in mol per cent. In addition, the positions of the characteristic bands for the first- and second-derivative curves are denoted around 435 nm and 425 nm, respectively, with dash lines, which are marked with P_{435} and P_{425} . The amplitudes of these characteristic bands, measured as the difference between the minimum at the band and the next associated maximum at longer wavelength in the derivative curves are marked as I_{435} and I_{425} .

the goethite content in soils not containing iron oxides other than haematite at concentrations down to 5 g kg^{-1} (Scheinost *et al.* 1998; Torrent *et al.* 2007; Sellitto *et al.* 2009). It is apparent that a peak position shift occurs for samples with different Al content (Fig. 3).

The DRS parameters (I_{435} , I_{425} , P_{435} , P_{425}) follow a slightly skewed normal distribution. In addition, the Kolmogorov–Smirnov test was carried out to prove the data distribution. The variables tested (the corresponding symbols are shown in Table 2) are normally distributed for all samples ($p > 0.05$). The average values and standard derivations are calculated based on the Gaussian distribution fitting, and the corresponding medium values are termed $I_{435,m}$, $I_{425,m}$, and $P_{435,m}$ and $P_{425,m}$, respectively (see the Appendix). The Al dependence of characteristic peak positions and amplitudes for each series samples are summarized in Fig. 4. Overall, $P_{435,m}$ and $P_{425,m}$ are negatively correlated with Al content, decreasing to lower wavelength with the increasing of Al content, which is similar to the Al dependence of P_{535} and P_{580} (the characteristic peaks for haematite) of haematite (Liu *et al.* 2011; Figs 4a and c). $I_{435,m}$ and $I_{425,m}$ first increase with Al content, reach a plateau for Al content in the 4–16 mol per cent range and then decrease with Al content increasing (Figs 4b and d). Therefore, the incorporation of Al into the structure of goethite plays an important role in controlling the DRS properties of goethite.

3.3 Results of magnetic measurements

The temperature dependences of magnetic susceptibility ($\chi-T$) are shown in Figs 5(a) and (b). The $\chi-T$ curve for the sample GtIII0 first decreases as temperature increases, but exhibits a sharp increase

from 350 K to reach a peak around 370 K, which is referred to as the Néel temperature (T_N) of goethite (Özdemir & Dunlop 1996; Mathé *et al.* 1999; Liu *et al.* 2006). Identical variations of $\chi-T$ curves can be observed for the other samples, but with lower peak temperature (also T_N) and wider peaks as Al content increases. In addition, both peak intensities and temperatures of series GtII* samples are lower than those of series GtIII* samples (Figs 5a and b), which demonstrates that T_N is markedly sensitive to the Al substitution and the synthetic procedure.

Thermal remanent magnetization (TRM) was calculated as the difference of FC and ZFC curves ($\text{TRM} = M_{\text{FC}} - M_{\text{ZFC}}$) to obtain the blocking temperature (T_b) of goethite (Liu *et al.* 2004, 2006). T_b shifts to lower temperature with increasing Al content (Fig. 5).

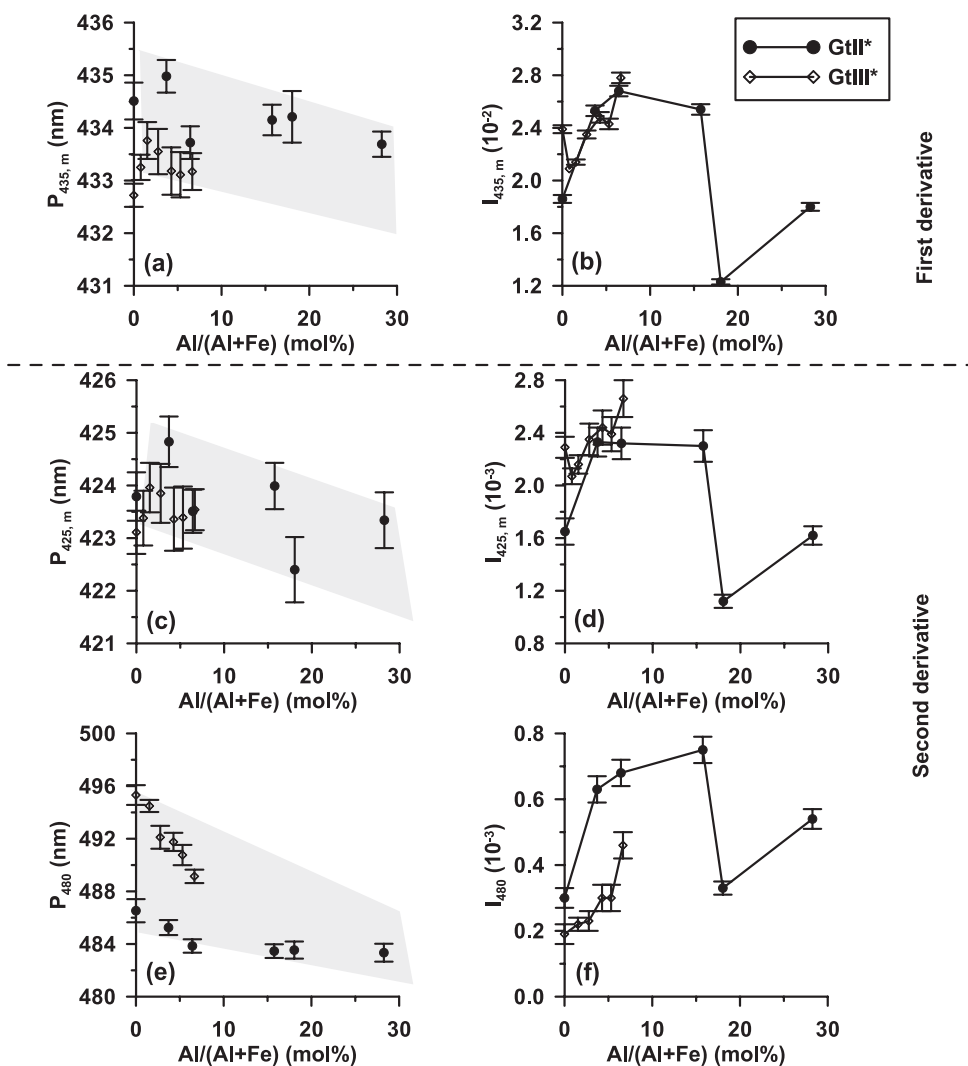
4 DISCUSSION

4.1 The mechanism of Al substitution influence on the DRS properties of goethite

The DRS spectra of Fe oxides exhibit several absorption bands in the UV-VIS range, which correspond to Fe^{3+} -crystal field transitions (Sherman & Waite 1985). Second-derivative spectra shows that the number and position of the absorption bands vary among the Fe oxides, thus the second-derivative spectra are used to diagnose different Fe oxides. The most prominent transitions that occur in the visible-UV range are: (1) a weak absorption band near $15\,000 \text{ cm}^{-1}$ (660 nm) corresponding to the $({}^6A_1) \rightarrow ({}^4T_2({}^4G))$ transition; (2) a marked band located near $19\,000\text{--}20\,000 \text{ cm}^{-1}$ (500–530 nm) corresponding to the electron pair transition (EPT), $2({}^6A_1) \rightarrow 2({}^4T_2({}^4G))$, which can be illustrated by the characteristic

Table 2. Notation of parameters used.

Parameter	Interpretation
T_N	Néel temperature
T_b	Blocking temperature
DRS	Visible diffuse reflectance spectroscopy
P_{435}	The position of minimum around 435 nm in the first-derivative curve of goethite DRS
P_{425}	The position of minimum around 425 nm in the second-derivative curve of goethite DRS
I_{435}	The amplitude at 435 nm in the first-derivative curve of goethite DRS
I_{425}	The amplitude at 425 nm in the second-derivative curve of goethite DRS
$P_{435,m}$	The medium value of P_{435}
$P_{425,m}$	The medium value of P_{425}
$I_{435,m}$	The medium value of I_{435}
$I_{425,m}$	The medium value of I_{425}
P_{535}	The position of minimum around 535 nm in the second-derivative curve of haematite DRS
P_{580}	The position of minimum around 580 nm in the first-derivative curve of haematite DRS
P_{480}	The position of minimum around 480 nm in the second-derivative curve of goethite DRS
I_{480}	The amplitude at 480 nm in the second-derivative curve of goethite DRS

**Figure 4.** The relationship between DRS parameters ($P_{435,m}$, $P_{425,m}$, $I_{435,m}$, $I_{425,m}$, P_{480} , I_{480}) and Al concentration of goethite, where the shaded areas in (a), (c) and (e) represent the variation trends of $P_{435,m}$, $P_{425,m}$ and P_{480} with Al content.

peak at 535 nm for haematite and 480 nm for goethite; and (3) a band near $23\,400\text{ cm}^{-1}$ (425 nm), observed only for goethite, corresponding to the (6A_1) \rightarrow (4E , 4A_1 (4G)) transition (Sherman & Waite 1985; Malengreau *et al.* 1994; Scheinost *et al.* 1998).

For goethite, previous studies paid most attention to the Al dependence of intensities (I_{480}) and positions (P_{480}) of the peak at 480 nm (Kosmas *et al.* 1986; Scheinost *et al.* 1999), the assignment of this band to the EPT, while detailed variations

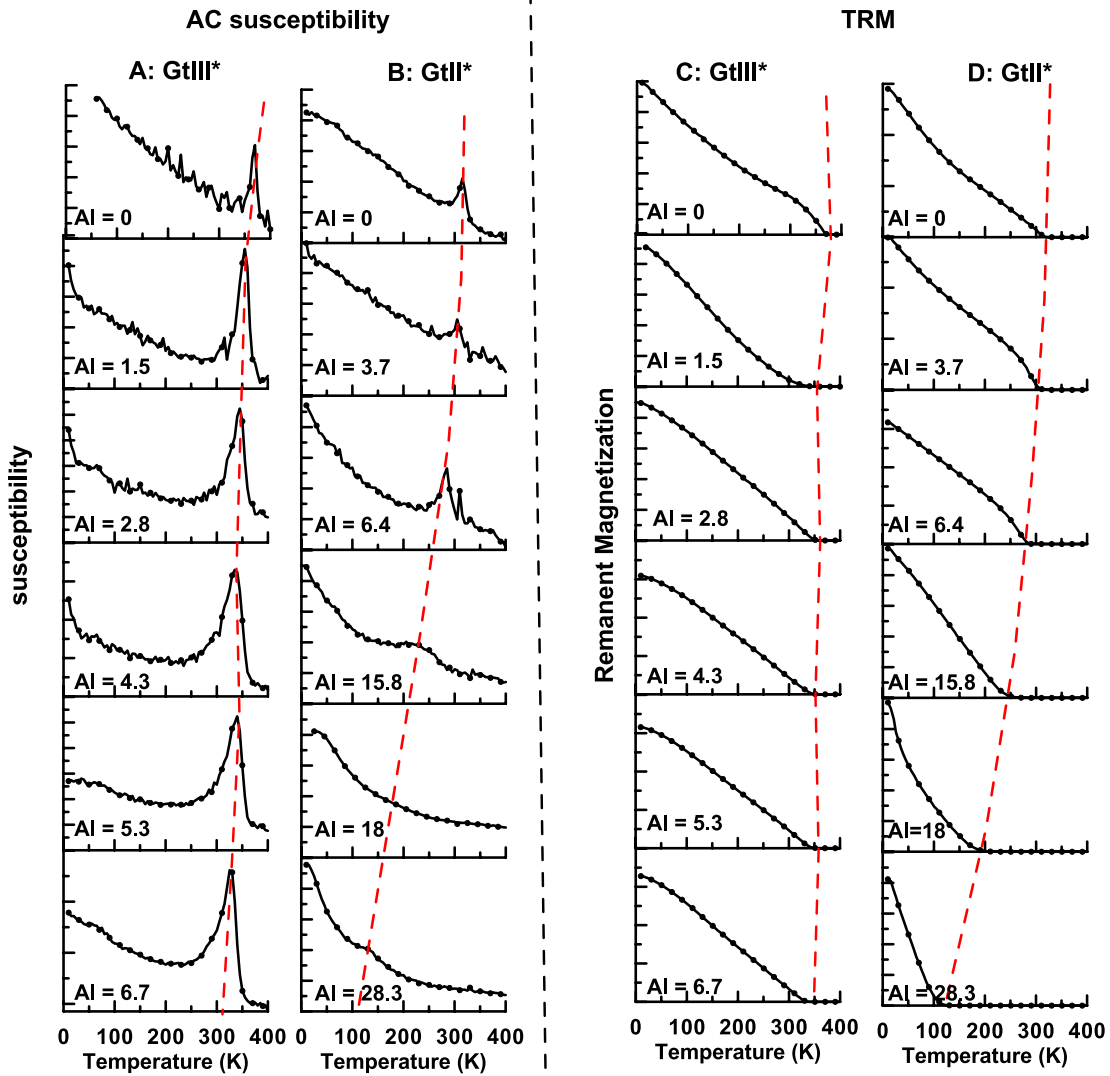


Figure 5. The temperature dependence of AC susceptibility and thermal remanent magnetization (TRM), where the red dash lines represent the shift of peaks. The number in every subplot represents Al content in mol per cent. Every column represents the same series samples.

occurring at 425 nm were ignored. However, both previous data (fig. 2 in Malengreau *et al.* 1994) and our results (Figs 3 and 4) show that peak position and amplitude of goethite at 425 nm in the DRS second-derivative curves are dependent on Al substitution. This phenomenon indicates that the position and energy of (6A_1) \rightarrow (4E , 4A_1 (4G)) transition band vary with Al content, which is in disagreement with previous findings (Kosmas *et al.* 1984, 1986; Scheinost *et al.* 1999). To compare the influencing mechanisms of Al substitution on these two band transitions, the variations of I_{480} and P_{480} with Al content were also calculated (Figs 4e and f). P_{480} varied negatively with Al content, as previous investigations proposed (Kosmas *et al.* 1986; Scheinost *et al.* 1999), moreover, I_{480} displayed a similar variation trend with I_{425} that it first increased and reached a maximum and then decreased as Al content increased. In addition, a clear separation of the two series samples can be observed for P_{480} and I_{480} . Therefore, the mechanism for the variation with Al content should be consistent for these two bands, because the variation of I_{425} and I_{480} with Al content is similar.

Al influences the DRS properties of goethite through two ways, crystal structure and particle size. The structure of goethite is com-

posed of $Fe(O,OH)_6$ octahedra, but a large number of $Al(O,OH)_6$ octahedra are formed during the incorporation of Al into the structure of goethite. Thus, the incorporation of Al into the structure will change the Fe^{3+} - Fe^{3+} magnetic coupling between face-sharing octahedra thereby increasing the EPT band energy and decrease the band intensity further (Kosmas *et al.* 1986; Scheinost *et al.* 1999). This is consistent with the variation mechanism of characteristic peak at 535 nm for haematite, assigned to the $2({}^6A_1)$ \rightarrow $2({}^4T_2({}^4G))$ transition (EPT) (Gálvez *et al.* 1999; da Costa *et al.* 2002; Torrent & Barrón 2003). In addition, the linkages of smaller $Al(O,OH)_6$ octahedra with those larger $Fe(O,OH)_6$ octahedra could give rise to substantial distortions. Distortions of the octahedra alter the Fe-(OOH) distances and lower the symmetry, which in turn alters the ligand field and shifts the band position (Sherman & Waite 1985; Burns 1993).

Meanwhile, the particle size of goethite can also change as a result of Al incorporation (Fig. 2), which may influence the DRS properties of goethite (Torrent & Barrón 2003). The correlations of these DRS parameters and the long-axis length are plotted in Fig. 6. It shows that $P_{435,m}$ is more sensitive to the long-axis length

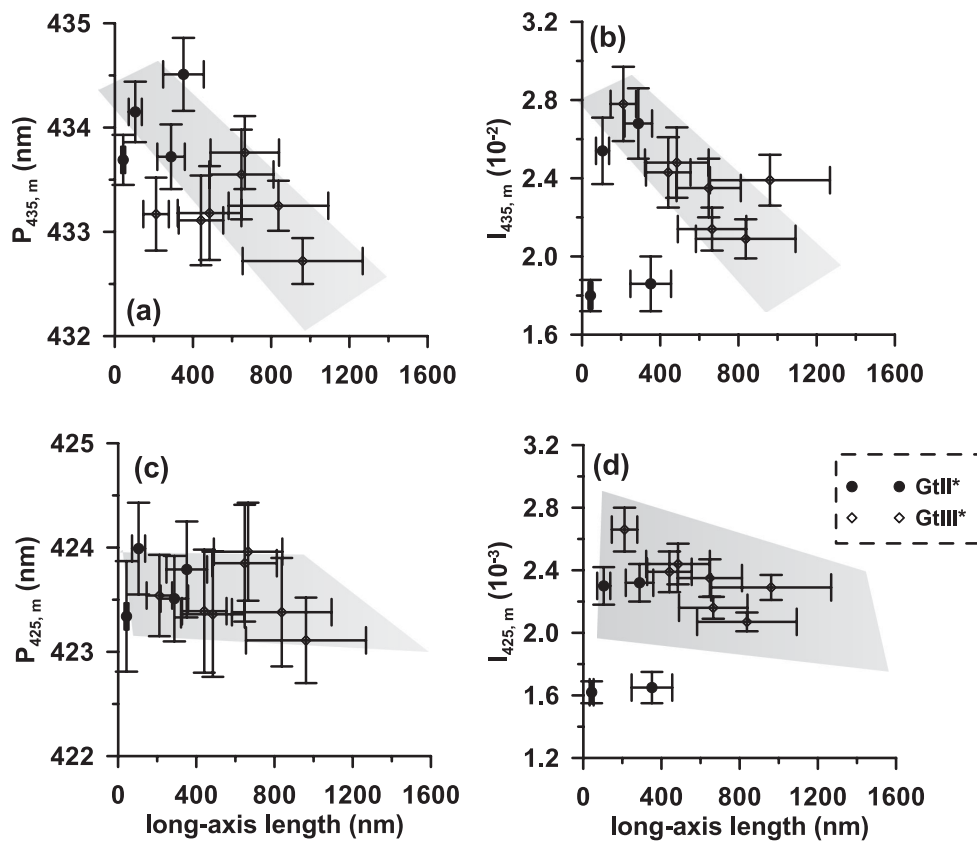


Figure 6. The relationship of DRS parameters ($P_{435,m}$, $P_{425,m}$, $I_{435,m}$, $I_{425,m}$) with the long-axis length of goethite particles, the shadow shapes indicate the variation trends for every diagram.

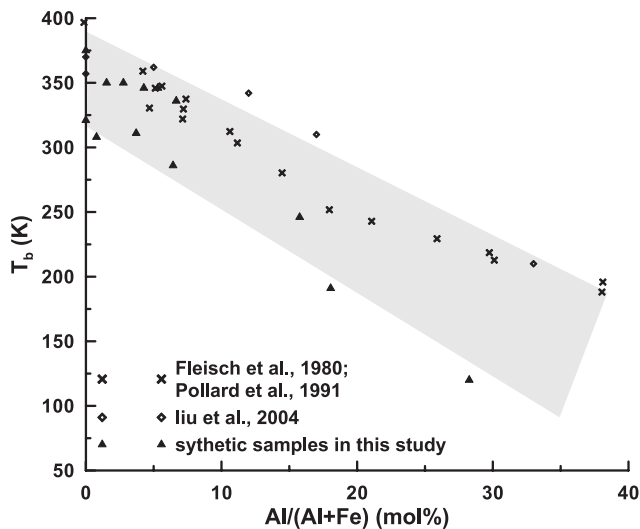


Figure 7. The diagram between Néel temperature (T_N) or blocking temperature (T_b) and Al substitution, where the solid triangle symbols stand for the T_N or T_b in this study, respectively, and the empty diamonds and crosses represent the data from Liu *et al.* (2004) and references therein.

than $P_{425,m}$, which is nearly independent of the long-axis length. In contrast, $I_{435,m}$ and $I_{425,m}$ vary significantly with the long-axis length, but the variation trend of $I_{435,m}$ (or $I_{425,m}$) versus long-axis length is distinctly different with that of $I_{435,m}$ (or $I_{425,m}$) versus Al content (Fig. 6). These results demonstrate that Al incorporation can influence the DRS properties of goethite by decreasing the long-axis length of goethite.

4.2 The feasibility of quantification of goethite with DRS

It is well known that the intensities of the bands at ~ 425 nm (I_{425}) and ~ 535 nm (I_{535}) are proportional to the concentration of goethite and haematite, respectively, and can thus be used to indicate the relative mass variations of goethite and haematite in soils (Scheinost *et al.* 1998). Kosmas *et al.* (1984) found that as goethite content increases, I_{425} increases independently with Al substitution. Then, the first and second derivatives of DRS are prevalently used to estimate the content of goethite and haematite in soils (Deaton & Balsam 1991; Torrent *et al.* 2007; Zhou *et al.* 2010). Scheinost *et al.* (1998) used I_{425} of goethite and I_{535} of haematite to estimate the haematite/goethite ratio, and proposed that the absolute proportions of the two minerals can be obtained. Torrent *et al.* (2007) built up empirical formulae to estimate the absolute proportions of haematite and goethite by the combination of I_{425} , I_{535} and the CBD extractable Fe content in stoichiometric haematite and goethite.

However, the influence of Al substitution on I_{425} and I_{535} cannot be ignored. Several studies have suggested that the incorporation of Al into the structure of iron oxides has taken a significant effect on the DRS properties of iron oxides (Kosmas *et al.* 1986). Liu *et al.* (2011) investigated several series of synthetic haematites ranging widely in the degree of Al substitution, and found that DRS properties of haematite are very sensitive to Al substitution, and a negative but non-linear correlation exists between band position of 535 nm (P_{535}), I_{535} and Al substitution, which should be considered when using I_{535} to estimate haematite content in soils.

Based on our statistical analysis, the amplitudes of characteristic bands in the first- and second-derivative curves of DRS are

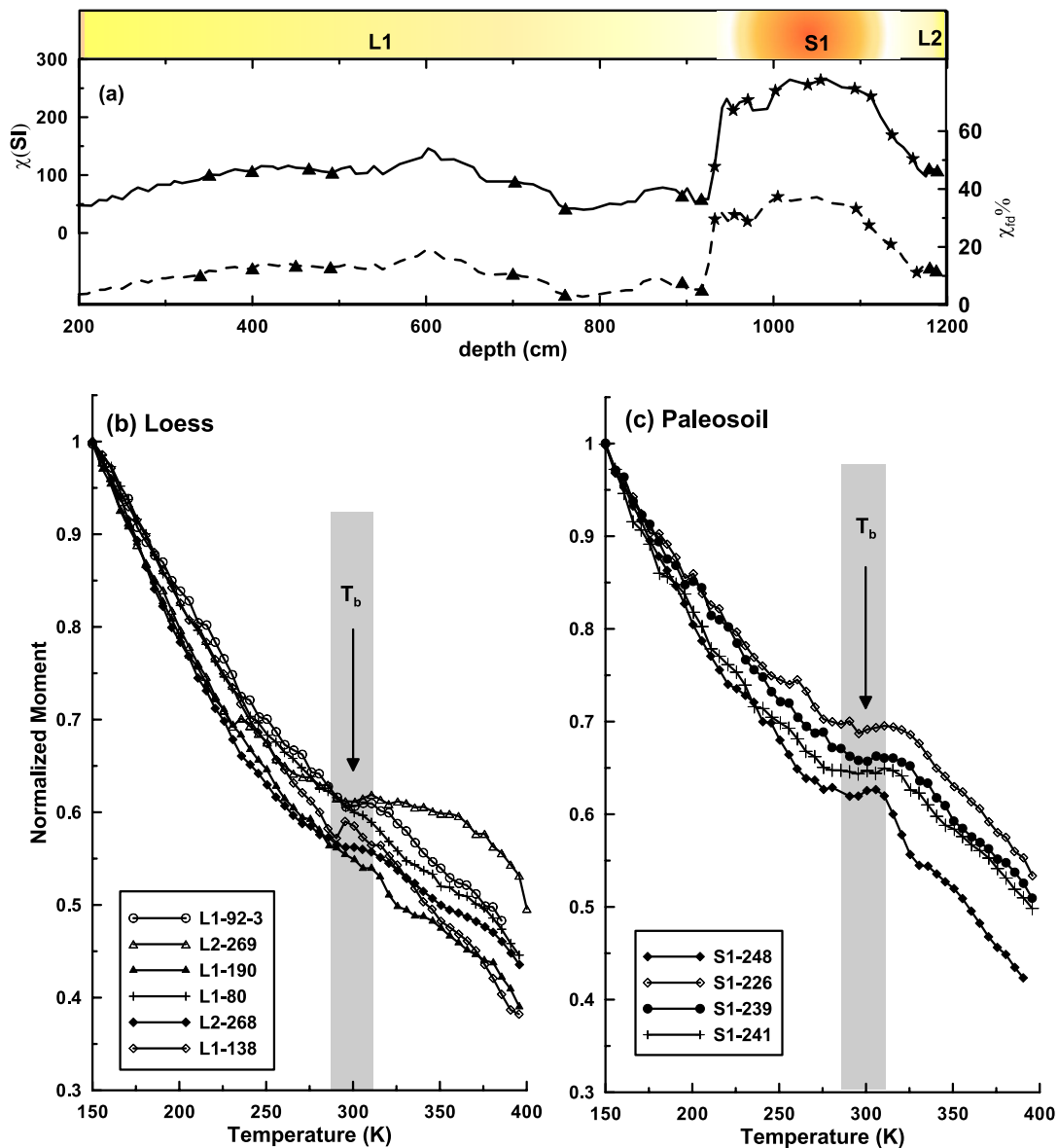


Figure 8. (a) The depth dependence of magnetic susceptibility (χ , solid line) and frequency susceptibility (χ_{fd} per cent, dash line) curves [revised from Hu *et al.* (2013)], and the solid triangle and solid star symbols represent the loess and palaeosol samples investigated in this study; (b and c) the temperature dependence curves of HIRM (hard IRM) for Chinese loess/palaeosol samples, the shadow areas indicating the blocking temperature of goethite.

very sensitive to Al substitution of goethite, and are constant only when Al substitution is between 4 and 16 mol per cent (Figs 4b and d). Therefore, it is less convincing to construct a function to translate band amplitude to absolute concentration of goethite without information on Al content. In addition, the amplitudes of characteristic bands are also different for goethite with different synthesis conditions, which should be considered when DRS data are used to quantify the content of goethite in soils. However, it is impractical to use the DRS parameters to estimate the Al substitution because of the non-linear and complicated relationship between the DRS parameters and the Al substitution. It is also difficult to directly measure the Al substitution of goethite in natural soils and sediments. Consequently, a proxy for the Al content is imperative.

This study proposed that magnetic properties can be used to reach this goal because the magnetic properties of Al-goethite are dependent on the particle size, crystal defect and crystal parameters,

which are controlled by Al substitution (Schulze 1984; Dekkers 1989; Liu *et al.* 2004, 2006). Thus, Al substitution can affect the magnetic properties of goethite. Combined with previous results, a negative correlation between T_N or T_b and Al substitution is apparent (Fig. 7). It can be hypothesized that the incorporation of Al into the structure decreases T_N or T_b of Al-goethite by increasing crystal defects and further diluting the magnetic interactions of adjacent layers or reducing grain size (Liu *et al.* 2004). The linear relationship of T_N or T_b for goethite with Al content indicates that T_N and T_b are sensitive to Al substitution, thus they can be used as the proxy for the Al content in Al-goethite.

In order to verify the practicality of the combination of DRS and magnetic methods for the quantification of goethite in natural samples, the DRS, HIRM $\sim T$ and χ_{fd} were measured on 20 loess/palaeosol samples. These samples are selected from the L1, S1 and L2 horizons of Luochuan profile, which are marked in the curve of magnetic susceptibility versus depth (Fig. 8a). HIRM $\sim T$

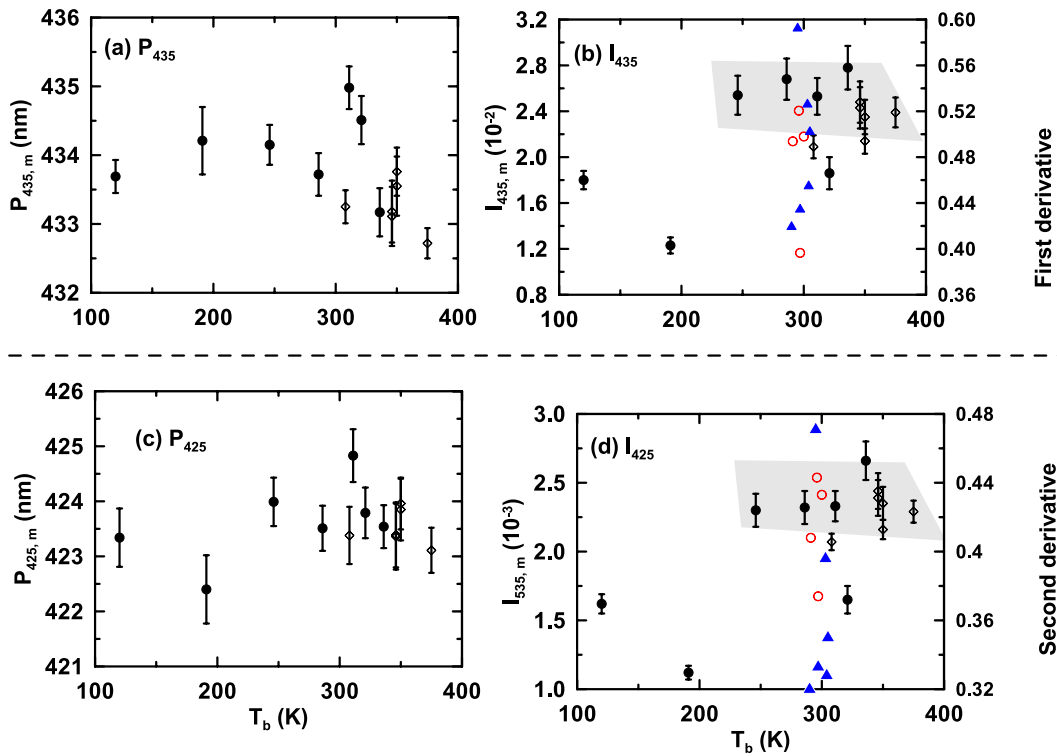


Figure 9. The relationship between DRS parameters ($P_{435,m}$, $P_{425,m}$, $I_{435,m}$, $I_{425,m}$) and T_b , where the solid circle and empty diamond represent series GtIII* and GtII* samples respectively; the shaded areas stand for the stable areas of $I_{435,m}$, $I_{425,m}$. In addition, the blue triangle and red empty circle symbols represent the loess and palaeosol samples, respectively.

curves (Figs 8b and c) show that HIRM decreases with temperature, and become stabilized at some temperature, which can be defined as T_b of goethite.

The T_b results of synthetic samples and these natural samples were plotted in the I_{425} (I_{435}) $\sim T_b$ diagrams (Fig. 9). It shows that $P_{435,m}$ is more sensitive to T_b (Fig. 9a), while $P_{425,m}$ is almost constant in the range of standard errors (Fig. 9c). However, both $I_{435,m}$ and $I_{425,m}$ are nearly constant when T_b is above 250 K, which suggests that T_b can be used as a parameter to define the stability of DRS intensity for goethite. For $T_b > 250$ K the DRS features are stable, that is, I_{435} and I_{425} may be used to estimate goethite content in soils and sediments, but it needs to be tested in soils. T_b for the loess/palaeosol samples is ~ 300 K, which suggests similar degree of Al substitution. Therefore, the DRS intensity variation between these samples should be attributed to differences in goethite concentrations; thus I_{435} and I_{425} can be used as the indicators of goethite content in natural samples. In addition, the loess and palaeosol samples are overlapped in the I_{425} (I_{435}) $\sim T_b$ diagram, indicating that goethite content is not controlled by pedogenesis process so distinctively like haematite.

In order to confirm this result, I_{553} and I_{535} , haematite content proxies, and χ_{fd} , an indicator for the concentration of pedogenic maghemite, were measured. Positive and significant correlations between I_{553} (I_{535}) and χ_{fd} (Figs 10b and d) are consistent with the hypothesis that maghemite is an intermediate product in the ferrihydrite to haematite transformation during pedogenesis (Barrón & Torrent 2002; Torrent *et al.* 2006; Torrent *et al.* 2007; Liu *et al.* 2008). However, I_{435} or I_{425} , proxies of goethite content, are independent of χ_{fd} , which should be attributed to the different formation processes of these two minerals. The formation of goethite is favoured in a soil environment that favours dissolution of ferrihydrite and further polymerization of the Fe^{3+} ions in solution (Cornell

& Schwertmann 2003), which is opposite to that of haematite and maghemite. So goethite content can be used to indicate a cold and moist climate, while haematite content is used for warm and seasonally dry environments (Balsam *et al.* 2004; Ji *et al.* 2004; Zhang *et al.* 2007). In addition, goethite in loess and palaeosols may be mainly controlled by detrital magnetic inputs; thus, there is no distinct correlation between I_{425} and χ_{fd} .

5 CONCLUSIONS

Two series of Al-goethites and some loess/palaeosol samples were investigated with DRS and magnetic methods. The peak position and amplitude of the DRS band for goethite were clearly influenced by Al substitution. The amplitude of the DRS band was stable only when Al substitution ranges between 4 and 16 mol per cent. Therefore, caution should be exerted when estimating the goethite content in soils and sediments from the amplitude of the DRS band. In order to resolve the difficulty in measuring Al content in natural samples, T_N or T_b was proposed as the new approach for estimating Al substitution of goethite. When T_b is above 250 K, DRS can be used to estimate goethite content in natural samples because the DRS intensity parameters are relatively independent of the Al content. For example, the DRS spectra for the Chinese loess–palaeosol samples support the idea that haematite is enhanced via pedogenesis. In contrast, the origin of goethite is mostly related to the aeolian inputs.

ACKNOWLEDGEMENTS

We thank Dr Zhifeng Liu, Caicai Liu and Qingqing Qiao for their valuable discussions. We are also grateful to Dr Jianli Zhang for his help about the DRS data processing. This study was supported by the

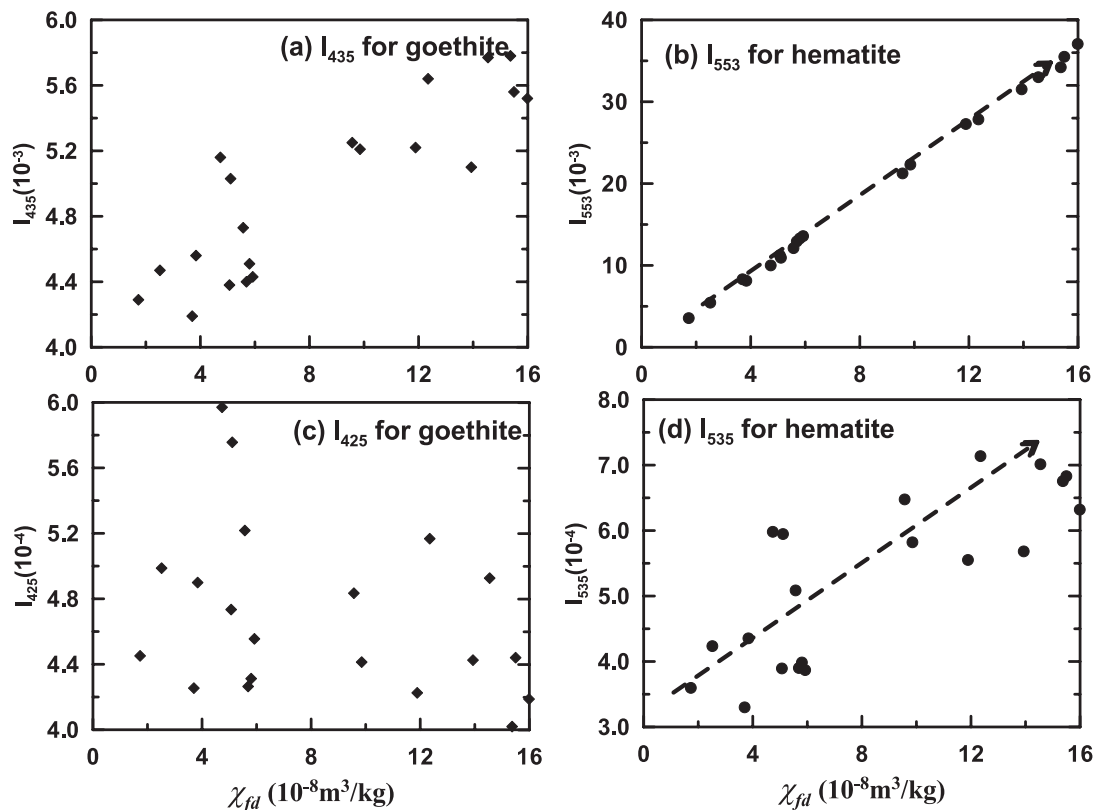


Figure 10. The diagrams between DRS parameters and χ_{fd} for Chinese loess/palaeosol samples. (a) I_{435} (goethite content proxy) versus χ_{fd} ; (b) I_{553} (haematite content proxy) versus χ_{fd} ; (c) I_{425} (goethite content proxy) versus χ_{fd} ; (d) I_{535} (haematite content proxy) versus χ_{fd} , where the dash lines in (b) and (d) indicate the variation trends for the diagrams.

National Natural Science Foundation of China (grants 41025013, 40974036 and 40821091). QSL acknowledges further support from the Chinese Academy of Sciences.

REFERENCES

- Balsam, W.L. & Deaton, B.C., 1996. Determining the composition of late quaternary marine sediments from NUV, VIS, and NIR diffuse reflectance spectra, *Mar. Geol.*, **134**, 31–55.
- Balsam, W.L., Ji, J. & Chen, J., 2004. Climatic interpretation of the Luochuan and Lingtai loess sections, China, based on changing iron oxide mineralogy and magnetic susceptibility, *Earth planet. Sci. Lett.*, **223**, 335–348.
- Banerjee, S.K., 1970. Origin of thermoremanence in goethite, *Earth planet. Sci. Lett.*, **8**, 197–201.
- Barrón, V. & Torrent, J., 1986. Use of the Kubelka–Munk theory to study the influence of iron oxides on soil colour, *Eur. J. Soil Sci.*, **37**, 499–510.
- Barrón, V. & Torrent, J., 2000. Evidence for a simple pathway to maghemite in Earth and Mars soils, *Geochim. Cosmochim. Ac.*, **66**, 2801–2806.
- Burns, R.G., 1993. Mineralogical applications of crystal field theory, in *Cambridge Topics in Mineral Physics and Chemistry*, 5th edn, eds Putnis, A. & Lieberman, R.C., Cambridge Univ. Press, pp 551.
- Cornell, R. & Schwertmann, U., 2003. *The Iron Oxides*, VCH Weinheim.
- da Costa, G.M., Van San, E., De Grave, E., Vandenberghe, R.E., Barrón, V. & Datas, L., 2002. Al hematites prepared by homogeneous precipitation of oxinates: material characterization and determination of the Morin transition, *Phys. Chem. Miner.*, **29**, 122–131.
- Deaton, B.C. & Balsam, W.L., 1991. Visible spectroscopy: a rapid method for determining hematite and goethite concentration in geological materials, *J. Sediment. Res.*, **61**, 628–632.
- Dekkers, M.J., 1989. Magnetic properties of natural goethite: I. Grain-size dependence of some low- and high-field related rock magnetic parameters measured at room temperature, *Geophys. J.*, **97**, 323–340.
- Dekkers, M.J. & Rochette, P., 1992. Magnetic properties of chemical remanent magnetization in synthetic and natural goethite: prospects for a natural remanent magnetization/thermoremanent magnetization ratio paleomagnetic stability test? *J. geophys. Res.*, **97**, 17 291–17 307.
- Evans, M.E. & Heller, F., 2003. *Environmental Magnetism: Principles and Applications of Enviromagnetics*, Academic Press.
- Gálvez, N., Barrón, V. & Torrent, J., 1999. Effect of phosphate on the crystallization of hematite, goethite, and lepidocrocite from ferrihydrite, *Clays Clay Miner.*, **47**, 304–311.
- Hao, Q., Oldfield, F., Bloemendal, J., Torrent, J. & Guo, Z., 2009. The record of changing hematite and goethite accumulation over the past 22 Myr on the Chinese Loess Plateau from magnetic measurements and diffuse reflectance spectroscopy, *J. geophys. Res.*, **114**, doi:10.1029/2009JB006604.
- Hu, P., Liu, Q., Torrent, J., Barrón, V. & Jin, C., 2013. Dynamic dissolution of magnetic iron oxides in Chinese loess and indication on pedogenesis, *Earth planet. Sci. Lett.*, **369–370**, 271–283.
- Ji, J., Balsam, W. & Chen, J., 2001. Mineralogic and climatic interpretations of the Luochuan loess section (China) based on diffuse reflectance spectrophotometry, *Quat. Res.*, **56**, 23–30.
- Ji, J., Balsam, W., Chen, J. & Liu, L., 2002. Rapid and quantitative measurement of hematite and goethite in the Chinese loess-paleosol sequence by diffuse reflectance spectroscopy, *Clays Clay Miner.*, **50**, 208–216.
- Ji, J., Chen, J., Balsam, W., Lu, H., Sun, Y. & Xu, H., 2004. High resolution hematite/goethite records from Chinese loess sequences for the last glacial-interglacial cycle: rapid climatic response of the East Asian Monsoon to the tropical Pacific, *Geophys. Res. Lett.*, **31**, doi:10.1029/2003GL018975.
- Jiang, Z., Liu, Q., Barrón, V., Torrent, J. & Yu, Y., 2012. Magnetic discrimination between Al-substituted hematites synthesized by hydrothermal and thermal dehydration methods and its geological significance, *J. geophys. Res.*, **117**, doi:10.1029/2011JB008605.

- Kämpf, N. & Schwertmann, U., 1983. Goethite and hematite in a climosequence in southern Brazil and their application in classification of kaolinitic soils, *Geoderma*, **29**, 27–39.
- Kilcoyne, S. & Ritter, C., 1997. The influence of Al on the magnetic properties of synthetic goethite, *Physica B: Condens. Matter*, **234**, 620–621.
- Kosmas, C., Curi, N., Bryant, R. & Franzmeier, D., 1984. Characterization of iron oxide minerals by second-derivative visible spectroscopy, *Soil Sci. Soc. Am. J.*, **48**, 401–405.
- Kosmas, C., Franzmeier, D. & Schulze, D., 1986. Relationship among derivative spectroscopy, color, crystalline dimensions, and Al substitution of synthetic goethites and hematites, *Clays Clay Miner.*, **34**, 625–634.
- Lázaro, F.J., Gutiérrez, L., Barrón, V. & Gelado, M.D., 2008. The speciation of iron in desert dust collected in Gran Canaria (Canary Islands): combined chemical, magnetic and optical analysis, *Atm. Env.*, **42**, 8987–8996.
- Lewis, D. & Schwertmann, U., 1979. The influence of aluminum on the formation of iron oxides. IV. The influence of [Al],[OH], and temperature, *Clays Clay Miner.*, **27**, 195–200.
- Liu, Q., Barrón, V., Torrent, J., Eeckhout, S.G. & Deng, C., 2008. Magnetism of intermediate hydromaghemite in the transformation of 2-line ferrihydrite into hematite and its paleoenvironmental implications, *J. Geophys. Res.*, **113**, B01103, doi:10.1029/2007JB005207.
- Liu, Q., Torrent, J., Yu, Y., Deng, C. & Banerjee, S., 2004. Mechanism of the parasitic remanence of aluminous goethite [α -(Fe, Al) OOH], *J. geophys. Res.*, **109**, doi:10.1029/2004JB003352.
- Liu, Q., Yu, Y., Torrent, J., Roberts, A., Pan, Y. & Zhu, R., 2006. Characteristic low-temperature magnetic properties of aluminous goethite [α -(Fe, Al) OOH] explained, *J. geophys. Res.*, **111**, doi:10.1029/2006JB004560.
- Liu, Q., Roberts, A.P., Torrent, J., Horng, C.-S. & Larrasoana, J.C., 2007. What do the HIRM and S-ratio really measure in environmental magnetism? *Geochem. Geophys. Geosyst.*, **8**, Q09011, doi:10.1029/2007GC001717.
- Liu, Q., Torrent, J., Barrón, V., Duan, Z. & Bloemendal, J., 2011. Quantification of hematite from the visible diffuse reflectance spectrum: effects of aluminium substitution and grain morphology, *Clay Miner.*, **46**, 137–147.
- Malengreau, N., Muller, J.P. & Calas, G., 1994. Fe-speciation in kaolins: a diffuse-reflectance study, *Clays Clay Miner.*, **42**, 137–147.
- Mann, S., Cornell, R. & Schwertmann, U., 1985. The influence of aluminium on iron oxides; XII, High-resolution transmission electron microscopic (HRTEM) study of aluminous goethites, *Clays Clay Miner.*, **20**, 255–262.
- Mathé, P.E., Rochette, P., Vandamme, D. & Fillion, G., 1999. Néel temperatures of synthetic substituted goethites and their rapid determination using low-field susceptibility curves, *Geophys. Res. Lett.*, **26**, 2125–2128.
- Murad, E. & Bowen, L.H., 1987. Magnetic ordering in Al-rich goethites: influence of crystallinity, *Am. Mineral.*, **72**, 194–200.
- Özdemir, Ö. & Dunlop, D.J., 1996. Thermoremanence and Néel temperature of goethite, *Geophys. Res. Lett.*, **23**, 921–924.
- Rochette, P., Mathé, P.-E., Esteban, L., Rakoto, H., Bouchez, J.-L., Liu, Q. & Torrent, J., 2005. Non-saturation of the defect moment of goethite and fine-grained hematite up to 57 Teslas, *Geophys. Res. Lett.*, **32**, doi:10.1029/2005GL024196.
- Scheinost, A., Chavernas, A., Barrón, V. & Torrent, J., 1998. Use and limitations of second-derivative diffuse reflectance spectroscopy in the visible to near-infrared range to identify and quantify Fe oxide minerals in soils, *Clays Clay Miner.*, **46**, 528–536.
- Scheinost, A.C., Schulze, D.G. & Schwertmann, U., 1999. Diffuse reflectance spectra of Al substituted goethite: a ligand field approach, *Clays Clay Miner.*, **47**, 156–164.
- Schulze, D., 1984. The influence of aluminium on iron oxides. VIII. Unit-cell dimensions of Al substituted goethites and estimation of Al from them, *Clays Clay Miner.*, **32**, 36–44.
- Schulze, D. & Schwertmann, U., 1984. The influence of aluminium on iron oxides: X. Properties of Al-substituted goethites, *Clays Clay Miner.*, **19**, 521–539.
- Schwertmann, U., 1987. Occurrence and formation of iron oxides in various pedoenvironments, in *Iron in Soils and Clay Minerals*, pp. 267–308, eds Stucki, J.W., Goodman, B.A. & Schwertmann, U., Springer.
- Schwertmann, U., 1993. Relations between iron oxides, soil color, and soil formation, in *Soil Color*, eds Bigham, J.M. & Ciolkosz, E.J., Soil Sci. Soc. Am. Spec. Publ. No. 31.
- Schwertmann, U. & Cornell, R.M., 2000. *Iron oxides in the laboratory*, Wiley.
- Sellitto, V., Fernandes, R., Barrón, V. & Colombo, C., 2009. Comparing two different spectroscopic techniques for the characterization of soil iron oxides: diffuse versus bi-directional reflectance, *Geoderma*, **149**, 2–9.
- Shen, Z.X. et al., 2006. Spectroscopic analysis of iron-oxide minerals in aerosol particles from northern China, *Sci. Total Environ.*, **367**, 899–907.
- Sherman, D.M. & Waite, T.D., 1985. Electronic spectra of Fe³⁺ oxides and oxide hydroxides in the near IR to near UV, *Am. Mineral.*, **70**, 1262–1269.
- Taylor, R. & Schwertmann, U., 1978. The influence of aluminum on iron oxides. Part I. The influence of Al on Fe oxide formation from the Fe (II) system, *Clays Clay Miner.*, **26**, 373–383.
- Thompson, R. & Oldfield, F., 1986. *Environmental Magnetism*, Allen and Unwin, 227 pp.
- Torrent, J. & Barrón, V., 2002. Diffuse reflectance spectroscopy of iron oxides, *Encyclopedia. Surf. Coll. Sci.*, 1438–1446.
- Torrent, J. & Barrón, V., 2003. The visible diffuse reflectance spectrum in relation to the color and crystal properties of hematite, *Clays Clay Miner.*, **51**, 309–317.
- Torrent, J. & Barrón, V., 2008. Diffuse reflectance spectroscopy, in *Methods of Soil Analysis*, pp. 367–387, eds Ulery, A.L. & Drees, L.R., Soil Science Society of America.
- Torrent, J., Barrón, V. & Liu, Q., 2006. Magnetic enhancement is linked to and precedes hematite formation in aerobic soil, *Geophys. Res. Lett.*, **33**, L02401, doi:10.1029/2005GL024818.
- Torrent, J., Schwertmann, U., Fechter, H. & Alferez, F., 1983. Quantitative relationships between soil color and hematite content, *Soil Sci.*, **136**, 354–358.
- Torrent, J., Liu, Q., Bloemendal, J. & Barrón, V., 2007. Magnetic enhancement and iron oxides in the Upper Luochuan loess–paleosol sequence, Chinese Loess Plateau, *Soil Sci. Soc. Am. J.*, **71**, 1570–1578.
- Zhang, Y.G., Ji, J., Balsam, W.L., Liu, L. & Chen, J., 2007. High resolution hematite and goethite records from ODP 1143, South China Sea: co-evolution of monsoonal precipitation and El Nino over the past 600,000 years, *Earth planet. Sci. Lett.*, **264**, 136–150.
- Zhou, W., Chen, L., Zhou, M., Balsam, W.L. & Ji, J., 2010. Thermal identification of goethite in soils and sediments by diffuse reflectance spectroscopy, *Geoderma*, **155**, 419–425.

THE DISTRIBUTION OF P_{435} , I_{435} , P_{425} AND I_{425} MEASURED 30 TIMES FOR EVERY SAMPLE

In order to account for the variability in the diffuse reflectance spectrum (DRS) measurement due to differences in particle size orientation caused by differences in packing pressure, samples were poured out after one measurement, packed into the holder again and then tested. In total, each sample was measured 30 times. The positions of the characteristic bands for the first- (P_{435}) and second- (P_{425}) derivative curves are around 435 nm and 425 nm, respectively. Correspondingly, the amplitudes of these characteristic bands, measured as the difference between the minimum at the band and the next associated maximum at longer wavelength in the derivative curves (I_{435} , I_{425}) were calculated. Results show that the DRS parameters (I_{435} , I_{425} , P_{435} , P_{425}) follow a slightly skewed normal distribution (Figs A1 and A2). The average values and standard derivations were calculated based on the Gaussian normal distribution fitting, and the corresponding medium values are termed $I_{435,m}$, $I_{425,m}$, and $P_{435,m}$, $P_{425,m}$.

It is clear that $P_{435,m}$ shifts with the variation in Al content. More specifically, $P_{435,m}$ of the two series samples shifts to a longer wavelength and then to a shorter wavelength as Al content increases,

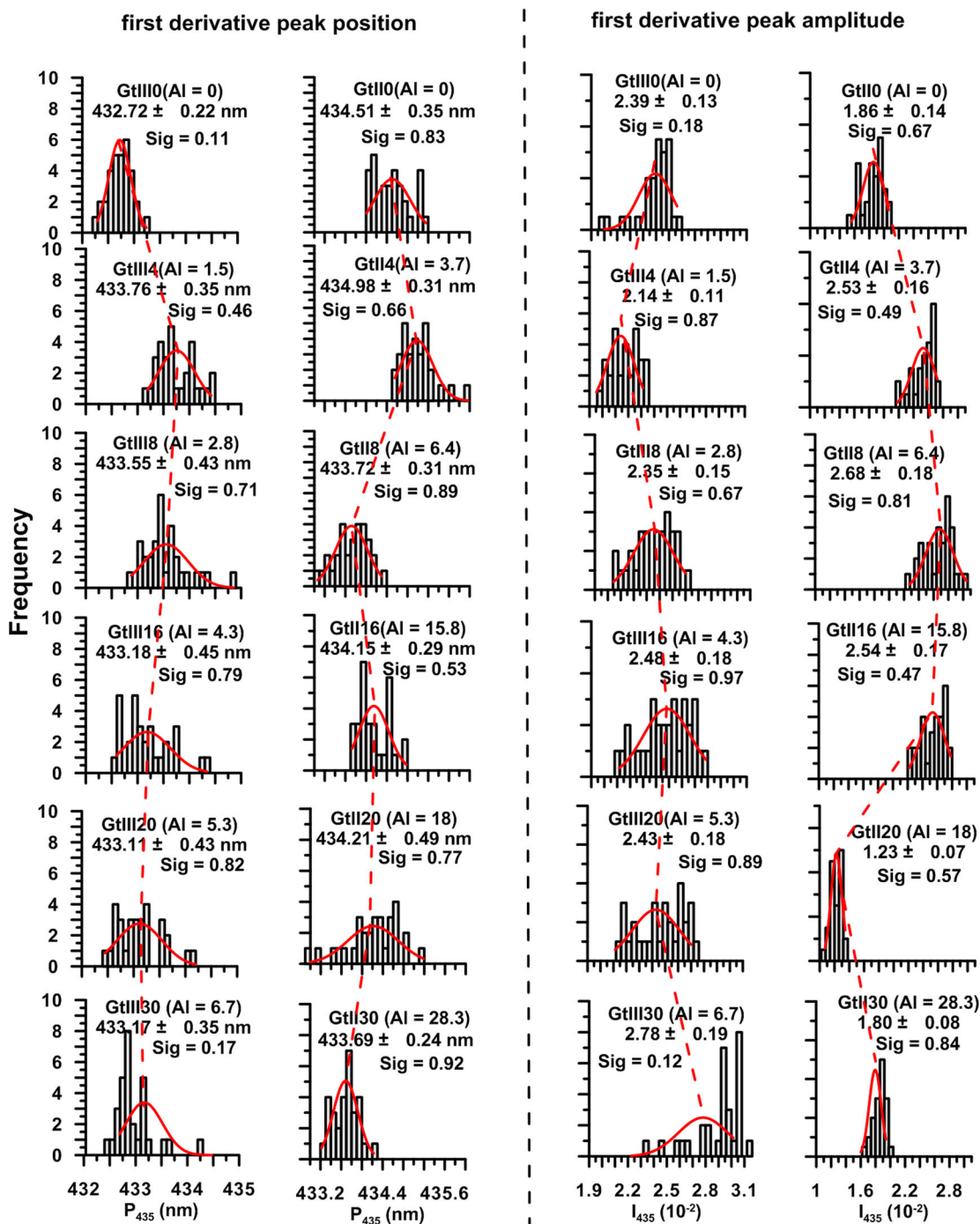


Figure A1. The distribution of P_{435} and I_{435} measured 30 times for every sample. The column represents the same series of samples, and red curves indicate the fitting curves for every distribution, and the red dash lines stand for the peak shift trend for every series samples. The number in the brackets indicates the final Al content in mol per cent. The values under samples names are mean values and standard deviations calculated based on the Gaussian distribution fitting curves. Moreover, the K-S normality tests were also carried out, and the test parameters *Sig* are shown in the graph.

and the peak positions for $I_{435,m}$ also shift to larger values first and then decrease to lower values concomitantly (Fig. A1). However, the variation for the parameters of the second-derivative curves

with Al content is not so clear, but the trend can still be observed that the peak positions of $P_{425,m}$ and $I_{425,m}$ shift to lower values as Al substitution increases (Fig. A2).

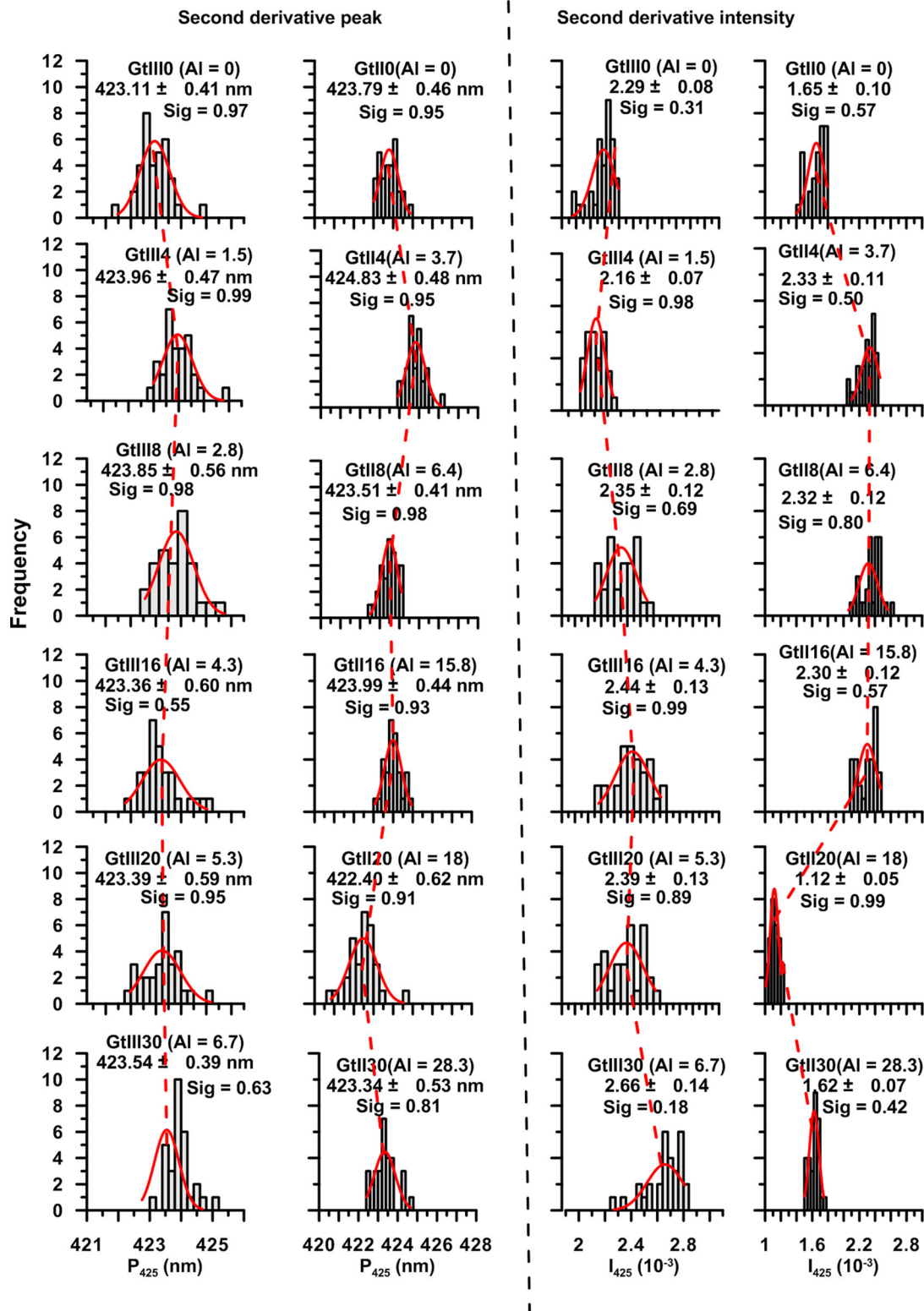


Figure A2. The distribution of P_{425} and I_{425} measured 30 times for every sample. Each column represents the same series of samples, and red curves represent the fitting curves for every distribution, and the red dash lines stand for the peak shift trend for every series samples. Numbers in the brackets are the final AI contents in mol per cent. The values under samples names are mean values and standard derivations calculated based on the Gaussian normal distribution fitting curves. Moreover, the K-S normality tests were also carried out, and the test parameter Sig are shown in the graph.